Machine-learning-based identification of influencing factors and synoptic patterns of foehn on the eastern foothills of the Taihang Mountains, China

Xinpeng Xu[1], Shoujuan Shu[1], Guochen Wang[1], Weijun Li[1]

[1]Department of Atmospheric Sciences, School of Earth Sciences, Zhejiang University, Hangzhou, 310058, China

Correspondence to: Dr. Shoujuan Shu (sjshu@zju.edu.cn)

Abstract. Foehn is generated over alpine terrain and is exerting increasingly pronounced impacts on air pollution, heatwaves, wildfires, and human health under global warming. Due to the complexity of influencing factors of foehn, it is difficult for traditional techniques to identify them, thereby limiting foehn's comprehensive assessments and accurate forecasting. Based on 64 years (1959–2022) of surface-station observations and reanalysis data, this study employs interpretable machine-learning techniques to systematically reveal the key controlling factors and dynamic thresholds of foehn on the eastern foothills of the Taihang Mountains, China. Results show that foehn formation is predominantly controlled by surface conditions and the influence of foehn factors varies seasonally: the leeward wind speed > 3 m/s from 203°–324° annually, the windward temperature below -17 °C in winter or 9 °C in summer, and the windward specific humidity > 0.07 g/kg in winter or 0.75 g/kg in summer. Synoptic analysis further reveals the weather patterns favorable for foehn occurrence, linking large-scale synoptic conditions with local thresholds for foehn formation. Foehn tends to occur under stable atmospheric stratification, with a surface high over the windward side and a low over the leeward side, together with an upper-level cold trough at 500 hPa and pronounced subsidence at 850 hPa on the leeward side on the eastern foothills of the Taihang Mountains. The findings further reveal that foehn occurrence is most favorable when the Froude number (Fr) over the Taihang Mountains falls between 0.82 and 1.5. Classical theory has only indicated that a Fr of approximately 1 favors foehn. This study, for the first time, extends this to a specific range, advancing the global understanding of foehn dynamics and offering a scientific basis for forecasting foehn and its associated compound disasters.

Keywords. machine learning; eastern foothills of the Taihang Mountains; foehn; influencing factors; synoptic patterns

1 Introduction

The term "foehn" originated from the name of a local wind over the European Alps. Nowadays, it is widely used in meteorology as a generic term to denote any warm and dry downslope wind descending from the leeward slope of a mountain range (Kusaka, Nishi et al. 2021). Foehn not only influences the local climatic environment of mountainous regions but can also cause a reduction in agricultural production (Lai 2018), exacerbate the spread of forest fires (Zumbrunnen, Bugmann et al. 2009), and exert adverse effects on air pollution conditions (Li, Jacob et al. 2020, Li, Ito et al. 2025) and human health (Liu, Lei et al. 2025, Schneidewind, Lee et al. 2025). Therefore, the foehn poses a significant challenge to the stability of mountain ecosystems and the sustainability of local socio-economic structures.

In the context of global warming, growing evidence showed that the intensity, frequency, and impact scope of foehn events are expanding globally. Foehn has been confirmed as a key mediator between global warming and cryospheric change. For example, the foehn caused regional warming along the eastern Antarctic Peninsula (Elvidge and Renfrew 2016), connected large-scale warming to Antarctic ice shelf evolution (Cape, Vernet et al. 2015), and triggered record-breaking

continental temperatures when coupled with atmospheric rivers (Bozkurt, Rondanelli et al. 2018). In mid-latitude regions, foehn and foehn-like phenomena have been considered as an important factor for the historic extreme temperature events, including the 74-year daily maximum temperature record revised in Japan in 2007 (Takane and Kusaka 2011). In fact, the risks of meteorological disasters are also increasing as the influences of foehn events extend in the past decade. Some studies showed that the intensified foehn-like events can exacerbate surface ozone pollution (Li, Jacob et al. 2020), trigger heatwaves (Ning, Yim et al. 2019) ,and increase wildfire risk (Zumbrunnen, Bugmann et al. 2009). Therefore, there are higher requirements for formation mechanisms of foehn and its operational forecasting. At present, it is critical to understand the foehn mechanisms, to clarify the key controlling factors of foehn occurrence and to improve its forecast accuracy in a warming world.

Previous studies have made some important progress on the foehn mechanism. The primary physical mechanism of foehn formation, the synoptic patterns and seasonal variability favorable to foehn occurrence have been identified (Elvidge and Renfrew 2016, Wiesner, McGowan et al. 2024). A range of frameworks to predict foehn events was developed in prior studies as well, including discriminant analysis-based foehn indices (Widmer 1966, Gutermann 1971, Jansing, Papritz et al. 2022), physical mechanism-based threshold methods (Ayitikan, Li et al. 2023), and decision tree-based classification approaches (Elvidge, Kuipers Munneke et al. 2020, Laffin, Zender et al. 2021, Francis, Fonseca et al. 2023). However, these methods commonly rely on manually selected thresholds, limiting their ability to resolve mixed atmospheric states or adapt to variable synoptic conditions (Stauffer, Zeileis et al. 2024). Although the automated identification methods have also been proposed (Plavcan, Mayr et al. 2014), they are highly dependent on high-temporal-resolution (ideally sub-hourly) in-situ measurements, which limits their promotion in regions with sparse observation networks (Stauffer, Zeileis et al. 2024). In addition, one forecasting framework based on numerical weather prediction (NWP) models can provide spatially continuous predictions, but are constrained by grid resolution, parameterization uncertainties, and inherent errors of the NWP models, preventing accurate capture of localized terrain-induced circulations (Grajek and Bednorz 2025, Maier, Klisho et al. 2025). In summary, previous studies have either been based on analyses of static foehn characteristics or relied on NWP numerical models, with few having objectively and quantitatively isolated the key predictors of foehn formation. To improve foehn prediction, multiple interpretable machine learning methods merit consideration for identifying its controlling factors.

To date, studying on the global foehn events focused on the classic mountain regions, including the Eastern Alps (Seibert 1990), Antarctica (Speirs, Steinhoff et al. 2010), the Andes (Seluchi, Norte et al. 2003), the Rocky Mountains (Beran 1967), the Toyama Plain in Japan (Kusaka, Nishi et al. 2021), and the southeastern Australia (Sharples, Mills et al. 2010). However, there was less typical work on the foehn events in the important mountain regions of China where it could be important for agriculture production, natural forest reservation, or close to large cities. Moreover, most studies on foehn in China primarily focused on the spatiotemporal characteristics analyses based on statistical methods (Shilin, Rongke et al.

1993, Huang 2011, Wang, Ding et al. 2012, Zhao, Li et al. 2021, Di, Zhang et al. 2022) and associated impacts of foehn (Chen and Lu 2015, Ning, Yim et al. 2019, Li, Jacob et al. 2020). Based on the complex topographic conditions and typical foehn phenomena in the Taihang Mountains (Shilin, Rongke et al. 1993, Wang, Ding et al. 2012, Di, Zhang et al. 2022), we noticed that the foehn events could occur frequently there, as an important geographical boundary between the second and third topographic steps of China. However, there is little in-depth investigation of the formation drivers and synoptic patterns of foehn in the Taihang Mountains.

In the Taihang Mountain region located in Northern China, the permanent population reaches 30.3 million, with Taiyuan and Shijiazhuang cities located on the windward and leeward sides, respectively. These two cities represent the two typical densely populated cities. As an important agricultural and industrial base in China, the Taihang Mountains are endowed with abundant natural, mineral, and tourism resources. What are the main factors influencing foehn formation? Do these factors exhibit thresholds and seasonal variations? How do these factors act within synoptic patterns to promote foehn occurrence? Addressing these questions is essential for better forecasting of foehn in populated complex-terrain regions, aiding disaster prevention, mitigation, and environmental protection.

2 Data and Methods

2.1 Study Area

The study area is the Taihang Mountain region in Northern China (Figure 1), with major cities including Taiyuan, the capital of Shanxi Province (the blue dot in Figure 1b, station elevation: nearly 800 m) and Shijiazhuang, the capital of Hebei Province (the middle red dot in Figure 1b, station elevation: 81 m). Topographically, the Taihang Mountains are one of China's most important mountain ranges, extending approximately 500 km in length and 40–50 km in width (Yusheng, 2010), roughly spanning 110–117°E and 35–41°N (the orange solid line in Figure 1b). They form a striking northeast–southwest oriented topographic barrier with steep eastern slopes facing the North China Plain and more gradual western slopes descending to the Loess Plateau. The average altitude of the mountains is 1,000 - 1,400 m, and the highest peak, Mount Wutai, which exceeds 3,000 m is located at the northern end of the Taihang Mountains (the northernmost tip of the orange solid line in Figure 1b). This pronounced topographic relief generates favorable conditions for foehn formation when moist air masses are forced to ascend the western slopes and descend adiabatically along the eastern leeward side.

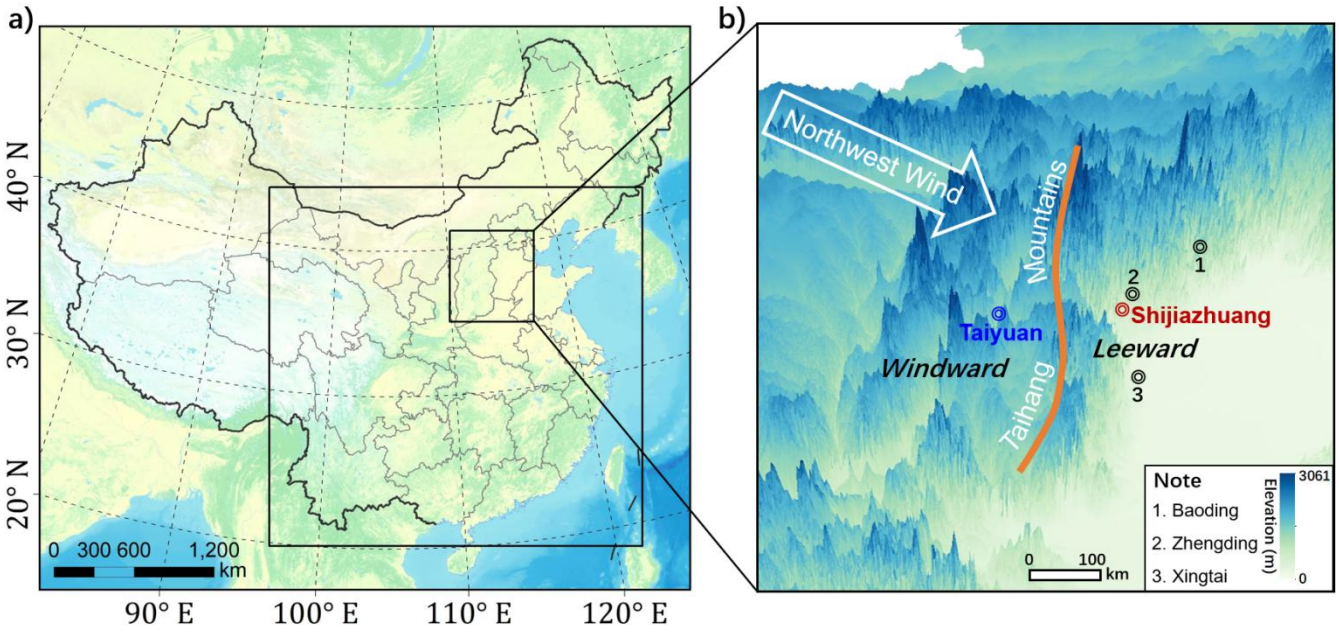

Figure 1: Regional map. (a) Major part of China (large black box) and the key area of foehn occurrence along the eastern foothills of the Taihang Mountains (small black box). (b) Geographical locations of meteorological stations in the region of Taihang Mountains, where blue and red dots indicate stations located on the windward and leeward sides, respectively.

2.2 Data and Processing

Meteorological data from five surface observation stations in the Taihang Mountain region (one located on the windward side and four on the leeward side; Figure 1b) were obtained from the National Oceanic and Atmospheric Administration (NOAA), covering a period of 64 years (1959–2022) with a temporal resolution of 3 hours. Corresponding upper-air data were acquired from the ERA5 reanalysis dataset of the European Centre for Medium-Range Weather Forecasts (ECMWF), with a spatial resolution of 0.25° × 0.25° and an hourly temporal resolution.

Since foehn occurs on the leeward slope, and the leeward stations vary in distance from the mountains, we compared the mean hourly temperatures during the main foehn season (winter, refer to Sect. 3.2) over the past 10 years (2012–2022) at the four leeward stations to select a representative site. The results show that Shijiazhuang and Xingtai, with closer proximity to the mountains, exhibit consistent diurnal variations, a pattern also observed in the more distant stations of Baoding and Zhengding. Moreover, the temperatures at stations closer to the mountains are higher than those at more distant stations (Figure S1). Therefore, Shijiazhuang, where is close to the mountains, exhibits more pronounced foehn characteristics and is densely populated, was selected as the representative leeward station, while Taiyuan was chosen as the windward station for subsequent analyses. For simplicity, the subscripts *Wind* and *Lee* are used below to denote the windward and leeward stations and their associated meteorological variables, respectively.

This study is limited to surface observations and lacks long-term upper-air data. To ensure the appropriate use of the high-resolution ERA5 reanalysis dataset, a comparative analysis was first performed with ground-based station measurements. Taking the average hourly surface temperature, humidity, and pressure during winter over the past 10 years

(2012–2022), the results (Figure S2) indicate that ERA5 grid data are slightly lower in magnitude than the station observations but exhibit highly consistent temporal variations, confirming the reliability of the ERA5 dataset. Therefore, this study will subsequently use 64 years of station observations and ERA5 reanalysis data to characterize surface and upper-air meteorological factors, respectively, for modeling and analysis.

2.3 Definition of foehn

Considering the local standard of Hebei Province and the foehn definitions proposed by Mony, Xiong, Kusaka, Aichinger-Rosenberger, Stauffer, and others (Mony 2020, Xianping, Shuyun et al. 2020, Kusaka, Nishi et al. 2021, Aichinger-Rosenberger, Brockmann et al. 2022, Stauffer, Zeileis et al. 2024), this study defines foehn events as summarized in Table 1.

Table 1: Definition of foehn events on the eastern foothills of the Taihang Mountains, China.

Definition Criteria	Explanation
Potential temperature ($\boldsymbol{\theta}$) difference $\boldsymbol{\Delta\theta > 2K}$	$\theta_{Lee} - \theta_{Wind} > 2K$, where $\theta = T(\frac{1000}{P})^{0.286}$
Relative humidity (Rh) difference $\boldsymbol{\Delta Rh > 20\%}$	$Rh_{Lee} - Rh_{Wind} <- 20\%$
Wind direction (Dir) $\boldsymbol{Dir = [WSW, WNW]}$	$Dir_{Lee} = [WSW, WNW] \cap Dir_{Wind} = [WSW, WNW]$ Wind directions on the windward and leeward sides occur within the WSW (West-Southwest) to WNW (West-Northwest) range.
Wind speed (W) $\boldsymbol{W > 2m/s}$	$W_{Lee} > 2m/s \cap W_{Wind} > 2m/s$ Wind speeds on the windward and leeward sides both faster than 2m/s.

2.4 Model Comparison

After cleaning and preprocessing the station observations and ERA5 reanalysis data, machine learning methods were employed to analyze the main influencing factors of foehn events on the eastern foothills of the Taihang Mountains. Six machine learning models were selected for this task: 1) K-Nearest Neighbor Classification (KNN), classifies samples based on the majority class among their k closest neighbors in the feature space (Cover and Hart 1967); 2) Logistic Regression, estimates the probability of class membership using a logistic function to model the relationship between input features and the binary outcome (Kleinbaum 2010); 3) Neural Network (NN), learns hierarchical representations through interconnected layers of neurons that apply nonlinear transformations to capture complex patterns in the data (Krizhevsky, Sutskever et al. 2017); 4) Decision Tree, recursively partitions the feature space into homogeneous regions based on feature values to make predictions (Salzberg 1994); 5) Random Forest (RF), is an ensemble method that constructs multiple decision trees using bootstrap sampling (bagging) and random feature selection at each split, and predictions are made by aggregating votes from

all trees, which reduces overfitting and improves generalization compared to single decision trees (Breiman 2001); 6) Adaptive Boosting (AdaBoost), sequentially trains weak learners, adjusting sample weights to focus on misclassified instances and combining their predictions through weighted voting to form a strong classifier (Freund and Schapire 1997). As our reviewing literature in the introduction, those conventional statistical methods struggle to analyze foehn formation due to the non-linear interactions among multiple atmospheric variables and the complex topographic modulation. These machine learning methods adopted in this study are able to automatically learn optimal decision boundaries and quantify factor importance via interpretable machine-learning techniques among the handling high-dimensional data and complex nonlinear relationships.

The preprocessed data were divided into training and testing sets, accounting for 70% and 30% of the total samples, respectively. The training set was used for model training with stratified 5-fold cross-validation, and hyperparameters were tuned to optimize model performance. Since the defined foehn samples were much fewer than the non-foehn samples, this study addressed the class imbalance issue by combining Synthetic Minority Over-sampling Technique (SMOTE) (Chawla, Bowyer et al. 2002), Random Undersampling method (Liu and Tsoumakas 2020), and Class Weight method (Yan, Ding et al. 2017) before conducting model training.

Based on model performance and reliability metrics, the most suitable machine learning model was selected. The correlation matrix (Figure S3) shows that the correlation between individual environmental factors and foehn occurrence is very low (correlation coefficients generally < 0.07), indicating that the complex nonlinear relationship between environmental factors and foehn events may lead to the difficulty of modeling with traditional methods, thus justifying the use of machine learning in this study. Evaluation results of accuracy, precision, recall, and F1 score (Figure S4) indicate that only the decision tree model achieves values above 0.8 for all four metrics. The confusion matrix (Figure S5) reveals that, since the 0 label (non-foehn samples) far outnumbers the 1 label (foehn samples), relying on a single metric such as accuracy is insufficient to evaluate model performance, and metrics like precision must also be considered. Receiver Operating Characteristic (ROC) curves and Area Under the Curve (AUC) values (Figure S6) show that logistic regression, decision tree, random forest, and AdaBoost models all have AUC values above 0.95, with the ROC curves of decision tree, random forest, and AdaBoost closely approaching the top-left corner, indicating superior performance. Learning curves (Figure S7) reveal that the KNN model suffers from overfitting while logistic regression is underfitted (overfitted) when the sample size is less (greater) than 50,000. Although the neural network fits well, it exhibits large fluctuations and uncertainties. The models of random forest and AdaBoost perform well with large samples but poorly with small samples, whereas the decision tree model consistently performs well. Therefore, the decision tree model was chosen finally as the basis for this study. Subsequently, Shapley Additive Explanations (SHAP) values (Lundberg and Lee 2017) were applied to interpret the model results and reveal the key factors influencing foehn formation on the eastern foothills of the Taihang Mountains.

2.5 Selection of Influencing Factors

Based on the previous studies (Mony 2020, Kusaka, Nishi et al. 2021, Aichinger-Rosenberger, Brockmann et al. 2022, Stauffer, Zeileis et al. 2024), this study extracted a total of 28 meteorological factors from the windward and leeward sides of the Taihang Mountains over the 64-year period (1959–2022), including 10 surface variables and 18 upper-air variables (Table 2), to serve as predictors for training the machine learning models.

Table 2: The 28 meteorological factors used as input variables for the machine learning models.

	Leeward side	Windward side	Explanation
Surface factors	SLP_{Lee}	SLP_{Wind}	Sea level pressure
	T_{Lee}	T_{Wind}	Temperature
	W_{Lee}	W_{Wind}	Wind speed
	Dir_{Lee}	Dir_{Wind}	Wind direction
	Q_{Lee}	Q_{Wind}	Specific humidity
Upper-air factors	TG_{Lee}	TG_{Wind}	Temperature gradient between 850 and 500hPa, obtained by the slope from the linear regression
	$Q8_{Lee}$	$Q8_{Wind}$	Specific humidity at 850hPa
	$W8_{Lee}$	$W8_{Wind}$	Wind speed at 850hPa
	$Dir8_{Lee}$	$Dir8_{Wind}$	Wind direction at 850hPa
	$Q7_{Lee}$	$Q7_{Wind}$	Specific humidity at 700hPa
	$W7_{Lee}$	$W7_{Wind}$	Wind speed at 700hPa
	$Dir7_{Lee}$	$Dir7_{Wind}$	Wind direction at 700hPa
	$Z5_{Lee}$	$Z5_{Wind}$	Geopotential height at 500hPa
	$T5_{Lee}$	$T5_{Wind}$	Temperature at 500hPa
Label	Foehn		A foehn event occurred

3 Results

3.1 The dominant factors contributing to the formation of foehn

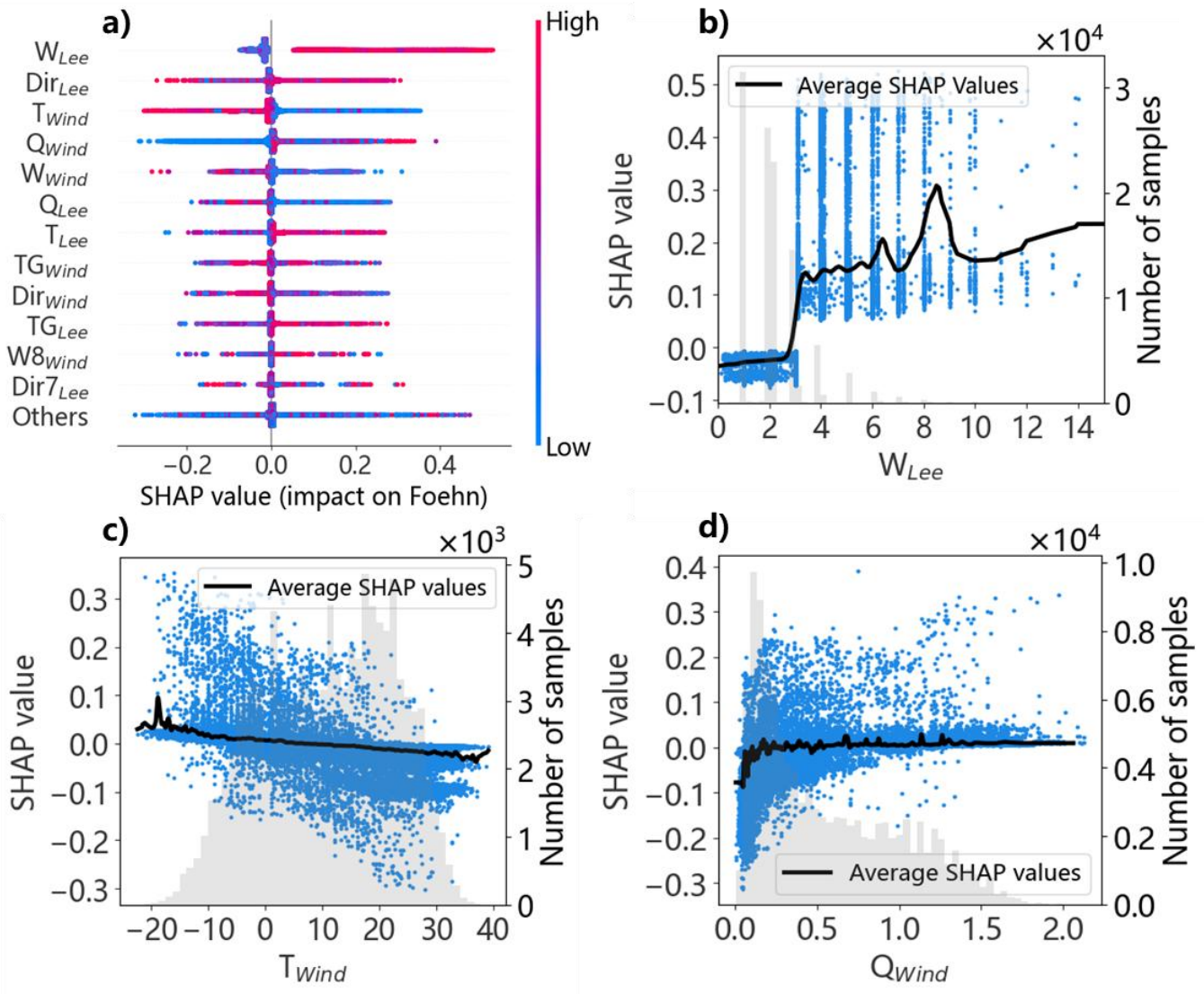

Figure 2: The dominant factors of foehn formation and their associated SHAP values revealed by interpretable machine-learning models. (a) SHAP summary plot, where the horizontal axis denotes SHAP values, individual dots represent samples, and dot color encodes the magnitude of the sample's feature value. (b) SHAP scatter plot for the leeward surface wind speed. (c) Same as (b) but for the windward 2-m temperature. (d) Same as (b) but for the windward surface specific humidity. In panels (b–d), the horizontal and vertical axes indicate the feature value and the SHAP value, respectively; dots denote individual samples, the grey histogram bars show sample counts, and the black curve traces the average SHAP values.

In this study, SHAP values are employed to quantify the contribution of each influencing factor to foehn formation. Across the entire year, we identified four most influential factors: W_{Lee}、Dir_{Lee}、T_{Wind}、Q_{Wind} (Figure 2a). Figure 2a further demonstrates that surface-related factors dominate the formation of foehn winds, whereas the contribution of upper-air factors is comparatively minor. The most influential upper-air factor, TG_{Wind}, only ranks eighth, demonstrating that foehn initiation and maintenance on the eastern Taihang foothills are governed primarily by near-surface processes.

W_{Lee} ranks first among all factors, indicating that elevated wind speeds on the leeward side strongly favor foehn formation or persistence. The SHAP scatter plot (Figure 2b) shows an abrupt increase in SHAP values from 0 to approximately 0.15 once W_{Lee} exceeds 3 m/s, signifying a sharp increase in foehn likelihood. The finding highlights 3 m/s of W_{Lee} as a critical threshold for the foehn formation. The average SHAP values curve (black line in Figure 2b) further exhibits a higher peak near 8 m/s, suggesting that this wind speed is even more conducive to foehn occurrence. The details are associated with seasons and discussed in Sect. 3.2,

The positive contribution of T_{Wind} decreases with increasing temperature (Figure 2c), implying that low-temperature conditions on the windward side facilitate foehn development. The average SHAP values curve crosses zero at 3°C (black line in Figure 2c), highlighting 3°C of T_{Wind} as a critical threshold for the foehn formation. As a result, the peak SHAP value around −18 °C suggests that such low temperature on the windward side are highly favorable for the foehn genesis.

In contrast, the SHAP mean for Q_{Wind} remains largely negative, denoting an overall inhibitory effect on foehn formation (Figure 2d). The curve crosses zero at roughly 0.1 g/kg (black line in Figure 2d), marking the threshold beyond which the inhibitory influence of Q_{Wind} becomes pronounced. The negative contribution weakens as Q_{Wind} increases, implying that the drier (lower specific-humidity) conditions on the windward side favor the foehn occurrence.

Comparing factors between the windward and leeward sides reveals that the same meteorological variables exert markedly different influences depending on location. For example, leeward wind speed influences foehn formation far more strongly than windward wind speed, because the accelerated subsidence of cross-mountain flow and its ability to reach the leeward stations constitute the foremost dynamical prerequisite for foehn formation. Conversely, the windward 2 m temperature and surface specific humidity exert stronger influences than the leeward 2-m temperature, underscoring that a cold, moist environment on the windward side favors the development of the foehn winds. Collectively, these results indicate that foehn occurrence requires a certain synoptic background that promotes dry-adiabatic descent of the cross-mountain flow, thereby warming and drying the leeward boundary layer and finally amplifying the surface foehn signal. The details are further examined in Sect. 3.3.

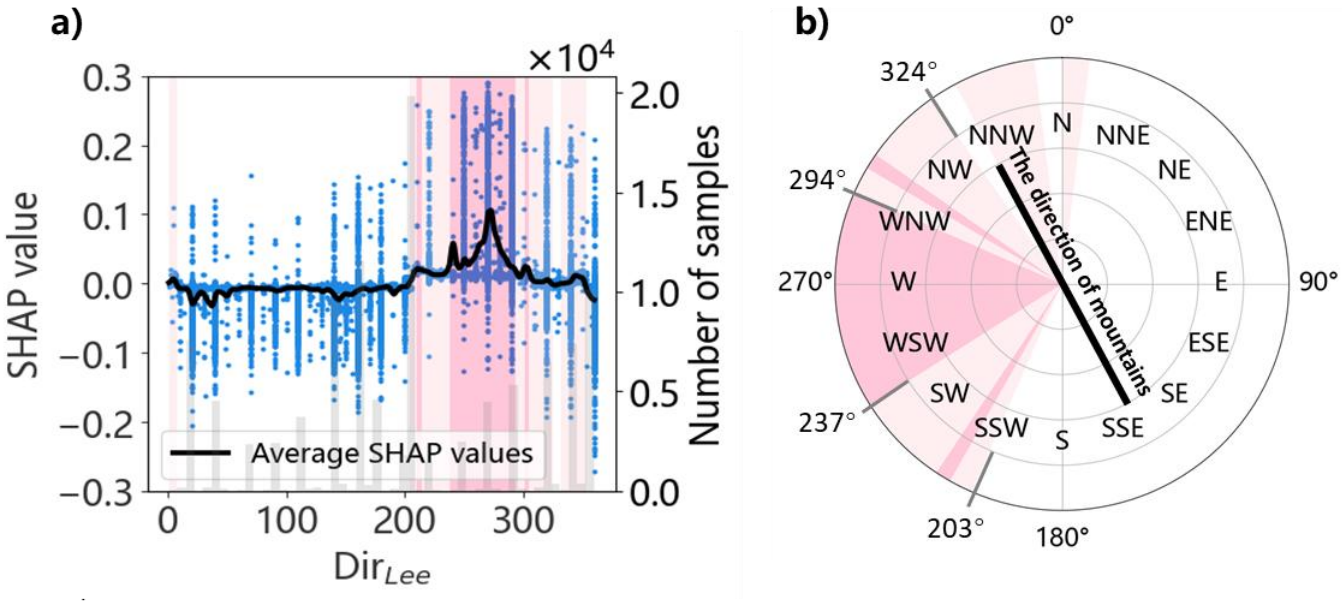

Figure 3: The role of the leeward surface wind direction and its contribution to foehn formation revealed by the interpretable machine-learning models. (a) SHAP-value scatter plot for the leeward surface wind direction. (b) Coordinate diagram of the leeward surface wind direction; the black straight line indicates the orientation of the central Taihang Mountains. In both (a) and (b), the shaded sectors correspond to each other: light pink shading denotes the positive-contribution with mean SHAP > 0, while rose red shading marks the largest positive mean SHAP values.

Dir_{Lee} is the second most influential factor for foehn occurrence on the eastern foothills of the Taihang Mountains (Figure 2a). Figure 3 shows the SHAP-based interpretable analysis for this factor. When Dir_{Lee} falls between 203° and 324° (the light-pink sector in Figure 3), the SHAP values are positive. This wind-direction range on the leeward side favors the foehn occurrence, and approximately 41 % of the samples fall within this positively contributing range (Figure 3a). Within the narrower sector 237° to 294° (rose-red shading in Figure 3), the positive contribution of the SHAP values further intensifies, signifying even more favorable conditions for the foehn formation. The average SHAP values curve (black line in Figure 3a) peaks when Dir_{Lee} equals 275°, revealing that a leeward wind direction of 275°, roughly 52° relative to the mountain axis, is most conducive to the foehn development in this region. Considering the relation between the positive contribution range (red shading in Figure 3b) and the orientation of the central Taihang Mountains (black line in Figure 3b), it becomes evident that the favorable wind directions are not strictly perpendicular to the ridge. Rather, foehn is more likely when the leeward wind makes a certain angle with the mountain range.

This wind-direction-dependent foehn formation mechanism is fundamentally supported by the Froude number (Fr) dynamics and terrain-airflow coupling effects, consistent with the principles of trans-barrier flow and orographic modification documented in foehn research (Durran 1990). Froude number, defined as $Fr = \frac{u}{Nh}$, (where u is the flow velocity normal to the topographic barrier, N is the Brunt-Väisälä frequency, and h is the height of the topographic barrier), quantifies the balance between inertial forces and buoyancy restoring forces, thereby determining the flow behavior when encountering topographic obstacles (Prósper, Sosa Tinoco et al. 2019, Wiesner, McGowan et al. 2024). When $Fr \ll 1$ there are significant

nonlinear effects and blocking, whereas for Fr≫1 the opposite occurs (Smolarkiewicz and Rotunno 1989, Smolarkiewicz and Rotunno 1990). The Fr around 1 indicates a transitional regime between the two states and favorable conditions for the formation of downslope lee windstorms and hydraulic jumps (Prósper, Sosa Tinoco et al. 2019, Wiesner, McGowan et al. 2024). Within this range, the airflow neither fully circumvents the range (Fr ≫ 1) nor is completely blocked (Fr ≪ 1), thereby sustaining a persistent downslope warming that favors foehn occurrence. Considering the u is the velocity of the flow normal to the topographic barrier, wind direction can be calculated or verified by aiming Fr (≈ 1) (Figure S8). Calculations show that the α (the angle between W_{Wind} and the mountain orientation) is equal to 41.81° and the wind direction is equal to 278.81°, which is really close the most conducive wind direction (275°) to the foehn development given by our SHAP method. Based on the obtained favorable wind direction (237°-294°, which means α = 33°-90°) identified in the SHAP model, the favorable Fr range is calculated as 0.82 to 1.5 for the formation of foehn on the eastern foothills of the Taihang Mountains. This finding not only agrees with classical theory but also extends it to a specific range for the first time, thereby enriching the global understanding of foehn dynamics. Such a result cannot be obtained from traditional theoretical studies.

Across all foehn cases examined here, approximately 56.4% (1473/2611) occurs when Dir_{Lee} lies within the optimal range of 237° to 294°. Seasonally, 42.3%（623/1473）of winter foehns and 9.2% (135/1473) of summer foehns fall within this favorable range, underscoring that the role of large-scale circulation patterns varies across seasons.

3.2 Seasonal variation of dominant foehn factors

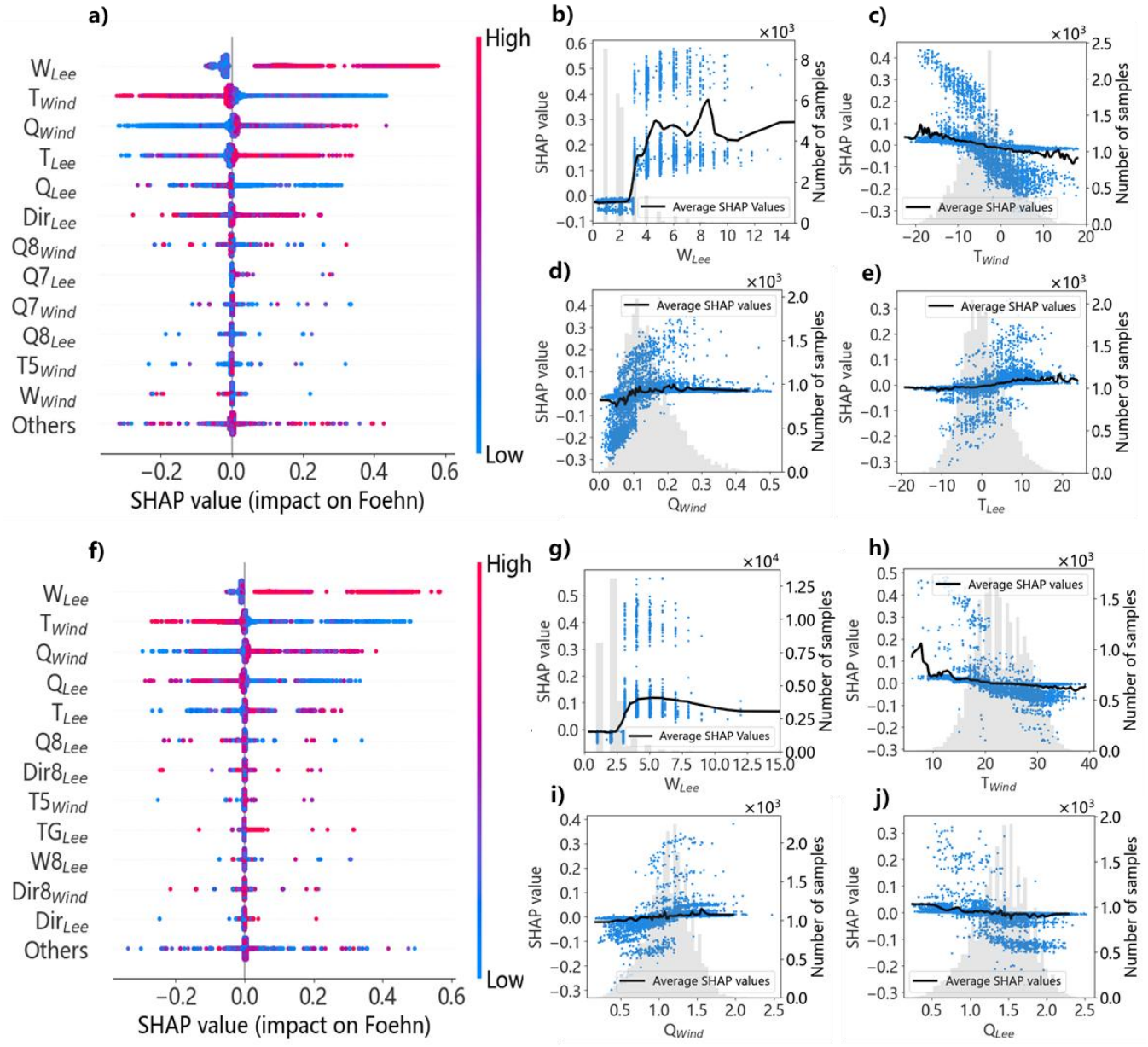

Figure 4: The seasonal dominant factors of foehn formation and their associated SHAP values revealed by interpretable machine-learning models. (a) SHAP summary plot for the key factors influencing winter foehn formation. (f) As in (a) but for summer. (b) SHAP scatter plot for the leeward surface wind speed in winter. (c–e) As in (b) but for the windward 2-m temperature, the windward surface specific humidity, and the leeward 2-m temperature in winter, respectively. (g) SHAP scatter plot for the leeward surface wind speed in summer. (h–j) As in (g) but for the windward 2-m temperature, the windward surface specific humidity, and the leeward surface specific humidity in summer, respectively.

To examine the seasonal dominant factors governing foehn formation on the eastern Taihang foothills, we re-trained models for winter and summer, respectively. The reason is that winter (December to February) is the peak season for haze and wildfire occurrences in North China (Zhang, Liu et al. 2020, Huang, Ding et al. 2023), and summer (June to August) is the key period drive the heat waves, ozone, and ultrafine particles (Li, Shao et al. 2020, Zhang, Xu et al. 2024). The result shows that the ranking of the leading factors is nearly identical in winter and summer, where W_{Lee}、T_{Wind}、Q_{Wind}

consistently occupy the top three positions (Figure 4a, f). Based on the fourth-ranking T_{Lee} in winter to Q_{Lee} in summer, we concluded that temperature becomes relatively more important in winter foehns, while humidity gained prominence in summer foehns. These three surface variables also dominate the annual SHAP ranking (Figure 2a), demonstrating that the leading role of surface factors is season-independent. On the annual scale, however, the leeward wind-direction factor (Dir_{Lee}) becomes more important. We noticed that the large-scale wind direction was mainly determined by the weather-scale circulation field. Therefore, the favorable synoptic circulations further modulated foehn occurrence by persistently influencing the leeward wind direction.

In addition to the seasonal differences in the dominant factors of the foehn wind, the influence thresholds and contribution strengths of specific factors also vary seasonally, which are summarized in Table S1. Figure 2b, Figure 4b and 4g reveal that W_{Lee} remains the overwhelmingly dominant factor in both seasons, with a universal threshold of 3 m/s. However, once this threshold is exceeded, the SHAP values in winter are markedly higher than those in summer, and a pronounced peak appears around 8.5 m/s in winter which is absent in summer (Figure 4b, g). The result indicates that the synoptic patterns conducive to high leeward wind speeds are more effective in triggering foehn events in winter than in summer.

In contrast to the influence of leeward wind speed, the temperature impacts become dominated by windward T_{Wind} rather than T_{Lee}. Positive contribution of T_{Wind} decreases monotonically with increasing temperature in both seasons (Figure 2c; Figure 4c, h), but the thresholds vary seasonally, being 3 °C annually, –6 °C in winter, and 9 °C in summer. Overall, the SHAP magnitudes are larger in summer, with a distinct peak near 7 °C that is absent in winter. As a result, a low windward temperature is more conducive to the foehn formation in summer than in winter.

The impacts of Q_{Wind} on foehn formation exceed that of Q_{Lee}, yet Q_{Wind} exerts a negative contribution in all seasons, with the inhibitory effect weakening as the humidity increases (Figure 2d; Figure 4d, i). The thresholds also vary seasonally, being 0.1 g/kg annually, 0.07 g/kg in winter, and 0.75 g/kg in summer. Overall, the SHAP magnitudes are larger in winter than in summer, which is opposite to the T_{Wind} pattern, demonstrating that a moist windward environment is more favorable for foehn development in winter than in summer.

3.3 Synoptic patterns associated with foehn occurrence

Xiong, Wang et al. (Xianping, Shuyun et al. 2020) noted that foehns on the eastern Taihang foothills are most pronounced in winter. Across the 2,611 foehn events identified during the 64 years in this study, 790 occurred in spring, 376 in summer, 558 in autumn, and 887 in winter, indicating that winter foehn events account for the largest proportion of the dataset. Our study also shows that winter foehn events also exhibit the longest persistence, which is up to 24 h, whereas in

the other seasons no event exceeds 6 h. Although previous studies documented the annual and seasonal variability of foehns (Xianping, Shuyun et al. 2020), the synoptic background conducive to their development remained unexamined.

We further define more precise winter foehn events on the eastern Taihang foothills simultaneously meeting the criteria in Sect. 2.3 and the thresholds (W_{Lee} > 3 m s^{-1}, T_{Wind} < −6 °C, Q_{Wind}> 0.07 g kg^{-1}, and Dir_{Lee} = 203°–324°) mentioned in Sect. 3.1 and 3.2. Using ERA5 reanalysis data spanning the most recent decade (2012–2022), we composited and analyzed the synoptic patterns favorable for foehn in winter on the eastern foothills of the Taihang Mountains (Figure 5).

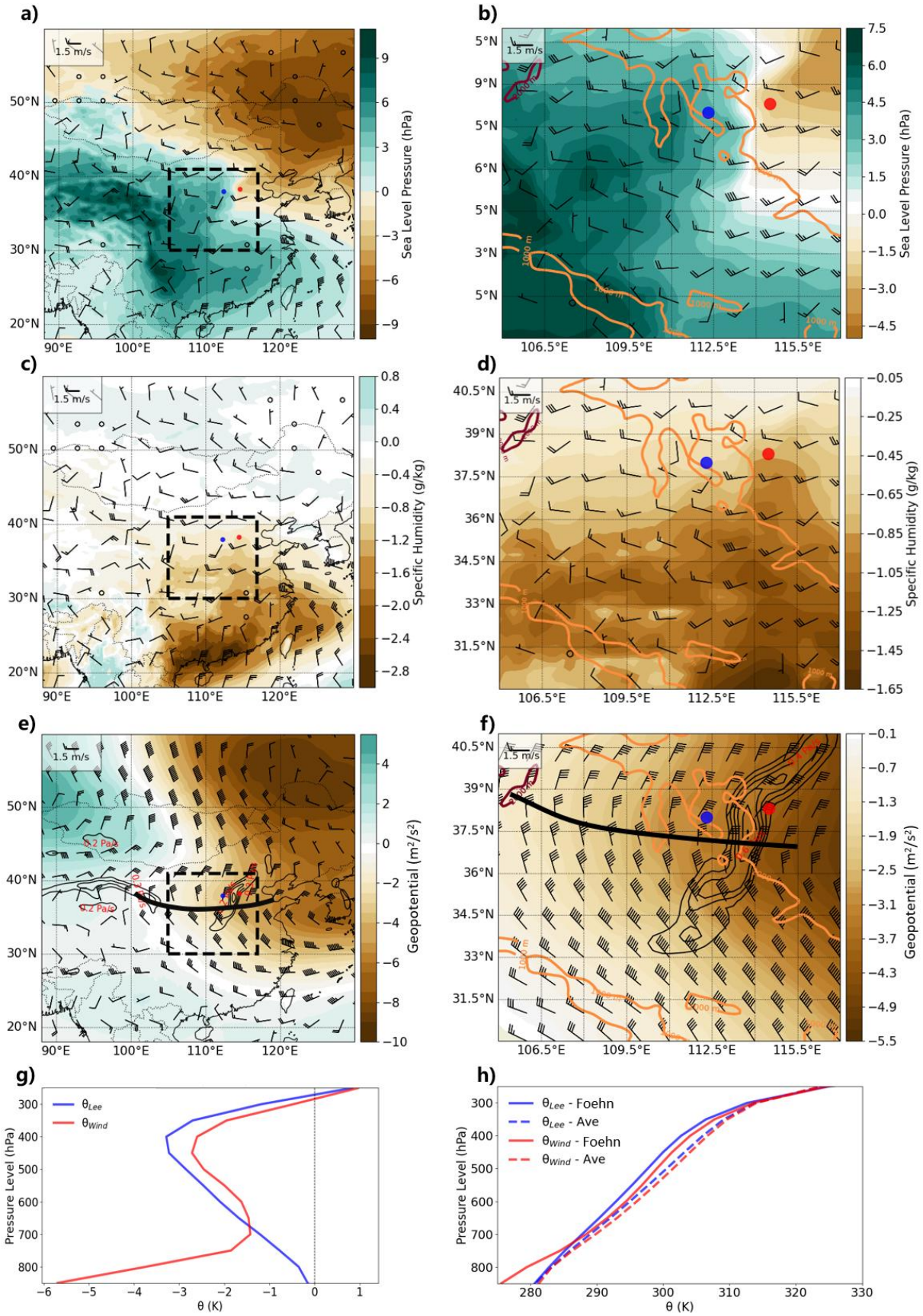

Figure 5: Anomalies of meteorological fields relative to the climatological mean during foehn events in winter on the eastern foothills of the Taihang Mountains: (a–b) Sea-level pressure (shaded) and 10 m wind field; (c–d) Surface specific humidity and 10 m wind field; (e–f) 500 hPa geopotential height (thick black contour denotes the westerly transverse trough), wind field, and 850 hPa vertical velocity (black contours, solid lines indicate subsidence); (g) Vertical profiles of potential temperature on the

windward and leeward sides. Blue and red dots mark the windward and leeward stations, respectively; the orange solid line indicates the position of the Taihang Mountains (defined by the 1,000 m elevation contour); the black dashed box in the left column outlines the domain shown in the right column. (h) Vertical profiles of potential temperature on the windward and leeward sides; "Foehn" and "Ave" denote the foehn events and the climatological mean, respectively.

Figure 5a, b display the winter-foehn anomalies in sea-level pressure (SLP) and 10 m wind relative to the climatological mean. It shows the zero-anomaly line (white contour) precisely transects the Taihang Mountains and the SLP was higher than climatological mean in southwest of the mountains (dark-green shading), accompanied by an anticyclonic (clockwise) wind shear on the synoptic scale. However, there was lower than climatological mean in the northeast (yellow shading), accompanied by cyclonic (counter-clockwise) wind (Figure 5a). Consequently, the region of Taihang Mountains is typically under a synoptic pattern featuring high pressure on the windward side and low pressure on the leeward side, accompanied by west-to-southwesterly upslope flow at the windward side (blue dots) and west-to-northwesterly downslope flow at the leeward side (red dots) (Figure 5b). This configuration favors the advection of warm and moist air masses which descend with sustained wind speed and thereby fosters foehn formation. The conclusion further confirmed the previous findings based on the SHAP method in Sect. 3.1.

Figure 5c, d display the surface specific-humidity anomalies. A pronounced dry anomaly extends northward from South China to the region of Taihang Mountains (Figure 5c). Although the entire mountain area is drier than climatology, the leeward side exhibits a sharp "upward bulge", forming the driest core at the same latitude (Figure 5d). The combination of downslope flow and the inherently dry leeward environment further amplifies the foehn warming drying signal on the leeward side. The synoptic analysis again corroborates the results in Sect. 3.1.

At 500 hPa (Figure 5e, f), a westerly cold trough (thick black line) is formed over the region of Taihang Mountains, with its low-pressure center situated on the leeward side (red dot) (Figure 5e). Strong northerly or north-easterly flow behind the trough drives vigorous subsidence on the leeward side (black contours in Figure 5f; maximum ≈ 0.7 Pa s^{-1}), supplying favorable dynamic conditions for the foehn formation through adiabatic warming during subsidence and downward momentum transfer.

Figures 5g, h reveal the atmospheric stratification stability through vertical potential-temperature (θ) profiles. The foehn events exhibit lower θ than the climatological mean between 700 and 300 hPa, with the largest deficit near 450 hPa on the leeward side (Figure 5h). This result shows that the presence of a mid-tropospheric cold air mass positively contributes to the foehn formation. Compared with climatology, the leeward side exhibits lower θ above 650 hPa, whereas the windward side shows a markedly lower θ within the 850–700 hPa lower troposphere (Figure 5g). It indicates that a pattern, which is colder in lower troposphere on the windward side and colder in upper layer on the leeward side, provides a stable atmospheric environment highly conducive to foehn events. In fact, both windward and leeward sides are within a stably stratified environment (θ increases with height) overall (Figure 5h). Previous results showed that the stable stratification inhibits

vertical mixing of the lower tropospheric airflow, leading to blocking of the cold air in the lower windward layer, while the warmer and drier air in the upper layer flows over the mountain and sinks along isentropic surfaces on the leeside (i.e., isentropic drawdown mechanism (Elvidge and Renfrew 2016, Wiesner, McGowan et al. 2024)). Also, the stable stratification provides favorable dynamic conditions for the development of mountain waves and hydraulic jumps (Wiesner, McGowan et al. 2024), which further accelerate the sinking of leeward airflow and enhance the foehn effects of temperature increase and humidity decrease. The large-scale environmental conditions we identified in Figure 5e, f further reveal the synoptic patterns responsible for the formation of stable stratification during foehn events in the Taihang Mountains, linking large-scale synoptic conditions with local foehn formation mechanisms and deepening the systematic understanding of foehn development.

In summary, foehns on the eastern Taihang Mountains preferentially occur in a stably stratified atmospheric environment with a surface pressure pattern characterized by a high- and low-pressure system on the windward and leeward sides, respectively. The foehn events are accompanied by an upper-level cold trough at 500 hPa and pronounced subsidence at 850 hPa on the leeward side.

4 Discussion and Conclusion

Based on the 64 years (1959–2022) of surface observations and ERA5 reanalysis data, and by integrating an interpretable machine-learning model with synoptic analysis, this study finds the dominant factors of foehn events on the eastern foothills of the Taihang Mountains as well as their spatiotemporal variability and its matched synoptic patterns.

Our study identifies W_{Lee}、Dir_{Lee}、T_{Wind}、Q_{Wind} as the four most influential factors for the foehn formation on the eastern Taihang foothills. In contrast to the previous reported foehn formation in Antarctica (Bozkurt, Rondanelli et al. 2018) or the Alps (Zumbrunnen, Bugmann et al. 2009, Aichinger-Rosenberger, Brockmann et al. 2022), which rely heavily on upper-level jets or atmospheric rivers, the Taihang foehn is governed almost exclusively by the surface factors and local topography, with upper-air contributes little. This result underscores a surface-dominated mechanism driven by local topography and the coupled surface wind–thermal system. Therefore, we recommend that the government should reinforce the weather monitoring stations along the eastern Taihang Mountain, prioritizing real-time observations of the leeward wind and of the windward temperature and specific humidity. Meanwhile, it is necessary to optimize the regional observation network so that more accurate inputs can be provided for foehn early warning systems.

By applying the SHAP-based explainable machine learning, we have quantified the critical dynamic thresholds for the foehn formation in this region and demonstrated their pronounced seasonal and spatial variability for the first time, instead of only setting fixed and empirical thresholds that lack seasonal and spatial adaptability (Widmer 1966, Elvidge, Kuipers Munneke et al. 2020, Laffin, Zender et al. 2021, Jansing, Papritz et al. 2022, Ayitikan, Li et al. 2023, Francis, Fonseca et al.

2023). The threshold of the leeward 10-m wind speed (W_{Lee}) remains stably above 3 m/s year-round, yet its contribution to foehn occurrence is significantly stronger in winter than in summer. Differently, the threshold of the windward 2-m temperature (T_{Wind}) is seasonally variable, being −10 °C annually, −17 °C in winter, and 9 °C in summer, with stronger impacts in summer than in winter. The windward specific humidity (Q_{Wind}) is predominantly suppressive and its thresholds are 0.1 g/kg annually, 0.07 g/kg in winter and 0.75 g/kg in summer, exerting a greater influence in winter than in summer. The thresholds of leeward wind-direction (Dir_{Lee}) are given as the favorable range from 203° to 324°, with the range from 237° to 294° being most conducive to foehn formation. Based on these findings, the Froude number (Fr) range most favorable for foehn occurrence in the Taihang Mountains is identified as 0.82 to 1.5. This result cannot be obtained through traditional theoretical methods alone. Classical theory has only indicated that a Fr of approximately 1 favors foehn. This study, for the first time, extends this to a specific range, advancing the global understanding of foehn dynamics. These thresholds can directly guide the development of seasonally and slope-resolved (windward versus leeward) differentiated early-warning models. For example, winter warnings should particularly target persistent strong foehns with an extended lead time (up to 24 h) and focus on leeward wind speeds (W_{Lee}) exceeding 3 m/s and windward specific humidity (Q_{Wind}) above 0.07 g/kg, while summer warnings should focus on windward temperature (T_{Wind}) below 9 °C (Figure 4).

Further analysis reveals that winter foehns not only account for 34% of annual events but also exhibit the longest durations (up to 24 h). These persistent episodes coincide with stable synoptic patterns that favor subsidence warming (Figure 5). Such conditions enhance low-level inversions and suppress boundary-layer ventilation, allowing pollutants to accumulate in a shallow surface layer and form a wintertime leeward haze layer (Gao, Zhang et al. 2015, Wang, Xue et al. 2015, Zhong, Zhang et al. 2019, Li, Shao et al. 2020). The severe haze pollution events in winter pose potentially severe health risks along the Taihang Mountain foothills. Consequently, winter alerts must pay particular attention to the superposition of foehn and stagnant weather.

Unlike the persistent haze pollution in winter, summer foehns act synergistically with heat waves and ozone episodes. Previous work shows that foehns can trigger anomalously hot and dry heat waves (Takane and Kusaka 2011), amplifying the surface radiative heating and accelerating the photochemical reactions (Li, Shao et al. 2020, Zhang, Xu et al. 2024, Zhou, Li et al. 2025), thereby causing rapid ozone accumulation. Summer foehn warnings should therefore monitor the coupled threshold of the rising temperature and plunging humidity on the leeward side to mitigate compound heat-ozone hazards. Moreover, the foehn's dry-hot signature sharply reduces humidity and elevates temperature on the leeward side, significantly increasing fire danger during the dry autumn–winter vegetation period (Zumbrunnen, Bugmann et al. 2009). Our study shows that westerly winds > 3 m/s during foehn events can further accelerate fire spread. An integrated "foehn–fire" monitoring and early-warning mechanism is therefore essential.

Composite analysis of winter foehn events, which dominate among different seasons, reveals the following favorable synoptic background: 1) A pronounced pressure gradient with higher pressure on the windward side and lower pressure on the leeward side drives westerly flow across the range; 2) the ambient air mass is cold and dry, whereas the leeward slope becomes markedly warm and dry; 3) a 500-hPa cold trough in the westerlies affects the leeward slope, inducing westerly or north-westerly downslope flow and pronounced subsidence in the lower troposphere (850 hPa); 4) the thermal structure is characterized by a stable stratification with colder air at low levels on the windward side and colder mid-upper levels on the leeward side. Therefore, priority should be given to the surface pressure gradient, the low-level vertical motion (especially subsidence), and the position of westerly troughs and ridges across the range of Taihang Mountains. Through identifying the specific synoptic patterns favorable for foehn occurrence in the Taihang Mountains, we link large-scale synoptic conditions with local thresholds for the formation of foehn in this study. This cross-scale physical connection and its mutual validation are difficult to achieve with conventional statistical methods alone. Therefore, we also recommend that when developing foehn-warning models, it is better to combine the surface thresholds with favorable synoptic-pattern information to construct a reliable "synoptic pattern plus surface factors" framework that overcomes the physical interpretability limitations of traditional single-model approaches (Seluchi, Norte et al. 2003, Stauffer, Zeileis et al. 2024).

Based on the findings above, here we recommend integrating the dynamic thresholds identified here into coupled meteorology-chemistry models to establish a unified "foehn–pollution–fire" monitoring and response system, thereby enhancing regional disaster prevention and climate-change resilience. In winter, the system should prioritize haze events triggered by continuous, intense foehn events that coincide with surface-based temperature inversions, and should extend the forecast horizon to 24 h. In summer, the focus shifts to foehn-triggered heatwaves and ozone pollution, with intensified joint monitoring of high temperature and low humidity on the leeward side. A dynamic fire-risk module also should be embedded, coupling foehn wind-speed and humidity thresholds with a vegetation dryness index to enable early detection and rapid response to natural hazards. Furthermore, our future study will further develop a regression model to predict specific foehn intensity metrics (e.g., foehn wind speed and warming magnitude), and reapply the SHAP interpretable method to quantify and reveal the key influencing factors governing these intensity indicators. These will serve as a useful reference for understanding foehn winds in other regions of the world.

Data Availability Statement

The NOAA station data is available at Hourly/Sub-Hourly Observational Data.

The ECMWF reanalysis data is available at ECMWF Reanalysis v5 | ECMWF.

Financial support

This study is supported by the National Natural Science Foundation of China (Grant No. U2442203 and 42375001).

Author contributions

S.S. and X.X. designed the study. X.X. conducted the research, including collecting the data, training the models and synoptic analysis. S.S. and X.X. interpreted the findings and wrote the first draft of the paper. G.W. provided support for the study area mapping. S.S., W.L. and X.X. contributed to the revision of the paper. All authors contributed to the discussion of the paper.

Competing Interest

We declare that the authors have no competing interests as defined by Nature Portfolio, or other interests that might be perceived to influence the results and/or discussion reported in this paper.

References

Aichinger-Rosenberger, M., E. Brockmann, L. Crocetti, B. Soja and G. Moeller (2022). "Machine learning-based prediction of Alpine foehn events using GNSS troposphere products: first results for Altdorf, Switzerland." Atmospheric Measurement Techniques 15(19): 5821-5839.

Ayitikan, M., X. Li, Q. He, Y. Musha, H. Tang, S. Li, Y. Zhong and G. Ren (2023). "Characteristics and Establishment of Objective Identification Criteria and Predictors for Foehn Winds in Urumqi, China." Atmosphere 14(8): 1206.

Beran, D. W. (1967). "Large Amplitude Lee Waves and Chinook Winds." Journal of Applied Meteorology and Climatology 6(5): 865-877.

Bozkurt, D., R. Rondanelli, J. C. Marin and R. Garreaud (2018). "Foehn Event Triggered by an Atmospheric River Underlies Record-Setting Temperature Along Continental Antarctica." Journal of Geophysical Research-Atmospheres 123(8): 3871-3892.

Breiman, L. (2001). "Random forests." Machine Learning 45(1): 5-32.

Cape, M. R., M. Vernet, P. Skvarca, S. Marinsek, T. Scambos and E. Domack (2015). "Foehn winds link climate-driven warming to ice shelf evolution in Antarctica." Journal of Geophysical Research-Atmospheres 120(21): 11037-11057.

Chawla, N. V., K. W. Bowyer, L. O. Hall and W. P. Kegelmeyer (2002). "SMOTE: synthetic minority over-sampling technique." Journal of artificial intelligence research 16: 321-357.

Chen, R. and R. Y. Lu (2015). "Comparisons of the Circulation Anomalies Associated with Extreme Heat in Different Regions of Eastern China." Journal of Climate 28(14): 5830-5844.

Cover, T. M. and P. E. Hart (1967). "Nearest Neighbor Pattern Classification." Ieee Transactions on Information Theory 13(1): 21.

Di, L., Q. Zhang, K. He, j. Sun and Z. Zhao (2022). "Analysis of Temporal and Spatial Characteristics of Foehn in Xingtai City." Journal of Agricultural Catastrophology 12(02): 122-124.

Durran, D. R. (1990). Mountain Waves and Downslope Winds. Atmospheric Processes over Complex Terrain. Boston, MA, American Meteorological Society: 59-81.

Elvidge, A. D., P. Kuipers Munneke, J. C. King, I. A. Renfrew and E. Gilbert (2020). "Atmospheric drivers of melt on Larsen C Ice Shelf: Surface energy budget regimes and the impact of foehn." Journal of Geophysical Research: Atmospheres 125(17): e2020JD032463.

Elvidge, A. D. and I. A. Renfrew (2016). "The Causes of Foehn Warming in the Lee of Mountains." Bulletin of the American Meteorological Society 97(3): 455-466.

Francis, D., R. Fonseca, K. S. Mattingly, S. Lhermitte and C. Walker (2023). "Foehn winds at Pine Island Glacier and their role in ice changes." The Cryosphere 17(7): 3041-3062.

Freund, Y. and R. E. Schapire (1997). "A decision-theoretic generalization of on-line learning and an application to boosting." Journal of Computer and System Sciences 55(1): 119-139.

Gao, Y., M. Zhang, Z. Liu, L. Wang, P. Wang, X. Xia, M. Tao and L. Zhu (2015). "Modeling the feedback between aerosol and meteorological variables in the atmospheric boundary layer during a severe fog–haze event over the North China Plain." Atmospheric Chemistry and Physics 15(8): 4279-4295.

Grajek, Z. and E. Bednorz (2025). "Climatology and circulation conditions of potential foehn occurrence in the Polish Tatra Mountains." Acta Geophysica 73(1): 955-967.

Gutermann, T. (1971). "Zur praktischen Anwendung des Föhntests von Widmer von Dr. Hans W. Courvoisier und."

Huang, X., K. Ding, J. Liu, Z. Wang, R. Tang, L. Xue, H. Wang, Q. Zhang, Z.-M. Tan, C. Fu, S. J. Davis, M. O. Andreae and A. Ding (2023). "Smoke-weather interaction affects extreme wildfires in diverse coastal regions." Science 379(6631): 457-461.

Huang, Y. (2011). "A Content Analysis of Newspaper Reports about Foehn Issues in Taiwan." World Regional Studies 20(04): 155-169.

Jansing, L., L. Papritz, B. Dürr, D. Gerstgrasser and M. Sprenger (2022). "Classification of Alpine south foehn based on 5 years of kilometre-scale analysis data." Weather and Climate Dynamics 3(3): 1113-1138.

Kleinbaum, D. G. a. K., M (2010). Logistic Regression: A Self Learning Text. New York, Springer.

Krizhevsky, A., I. Sutskever and G. E. Hinton (2017). "ImageNet Classification with Deep Convolutional Neural Networks." Communications of the Acm 60(6): 84-90.

Kusaka, H., A. Nishi, A. Kakinuma, Q.-V. Doan, T. Onodera and S. Endo (2021). "Japan's south foehn on the Toyama Plain: Dynamical or thermodynamical mechanisms?" International Journal of Climatology 41(11): 5350-5367.

Laffin, M., C. Zender, S. Singh, J. Van Wessem, C. Smeets and C. Reijmer (2021). "Climatology and evolution of the Antarctic Peninsula föhn wind-induced melt regime from 1979–2018." Journal of Geophysical Research: Atmospheres 126(4): e2020JD033682.

Lai, L. W. (2018). "The relationship between extreme weather events and crop losses in central Taiwan." Theoretical And Applied Climatology 134(1-2): 107-119.

Li, K., D. J. Jacob, L. Shen, X. Lu, I. De Smedt and H. Liao (2020). "Increases in surface ozone pollution in China from 2013 to 2019: anthropogenic and meteorological influences." Atmospheric Chemistry and Physics 20(19): 11423-11433.

Li, W., L. Shao, W. Wang, H. Li, X. Wang, Y. Li, W. Li, T. Jones and D. Zhang (2020). "Air quality improvement in response to intensified control strategies in Beijing during 2013–2019." Science of The Total Environment 744: 140776.

Li, W. J., A. Ito, G. C. Wang, M. K. Zhi, L. Xu, Q. Yuan, J. Zhang, L. Liu, F. Wu, A. Laskin, D. Z. Zhang, X. Y. Zhang, T. Zhu, J. M. Chen, N. Mihalopoulos, A. Bougiatioti, M. Kanakidou, G. H. Wang, H. L. Hu, Y. Zhao and Z. B. Shi (2025). "Aqueous-phase secondary organic aerosol formation on mineral dust." National Science Review 12(7).

Liu, B. and G. Tsoumakas (2020). "Dealing with class imbalance in classifier chains via random undersampling." Knowledge-Based Systems 192: 105292.

Liu, H., J. Lei, Y. Liu, T. Zhu, K. Chan, X. Chen, J. Wei, F. Deng, G. Li, Y. Jiang, L. Bai, K. Wang, J. Chen, Y. Lan, X. Xia, J. Wang, C. Wei, Y. Li, R. Chen, J. Gong, X. Duan, K. Zhang, H. Kan, X. Shi, X. Guo and S. Wu (2025). "Hospital admissions attributable to reduced air pollution due to clean-air policies in China." Nature Medicine 31(5): 1688-1697.

Lundberg, S. M. and S.-I. Lee (2017). "A Unified Approach to Interpreting Model Predictions." Advances in Neural Information Processing Systems (Nips 2017) 30(2): 847–856.

Maier, P., T. Klisho, H. Formayer and F. Lehner (2025). "Analysing the future trends of foehn-enabling synoptic patterns over two valleys in the Eastern Alps in CMIP5 EURO-CORDEX models." Theoretical and Applied Climatology 156(3): 155.

Mony, C. (2020). Evaluating foehn development in a changing climate using machine learning and investigating the impact of foehn on forest fire occurrence and severity, ETH Zurich.

Ning, G. C., S. H. L. Yim, S. G. Wang, B. L. Duan, C. Q. Nie, X. Yang, J. Y. Wang and K. Z. Shang (2019). "Synergistic effects of synoptic weather patterns and topography on air quality: a case of the Sichuan Basin of China." Climate Dynamics 53(11): 6729-6744.

Plavcan, D., G. J. Mayr and A. Zeileis (2014). "Automatic and probabilistic foehn diagnosis with a statistical mixture model." Journal of Applied Meteorology and Climatology 53(3): 652-659.

Prósper, M. A., I. Sosa Tinoco, C. Otero-Casal and G. Miguez-Macho (2019). "Downslope windstorms in the Isthmus of Tehuantepec during Tehuantepecer events: a numerical study with WRF high-resolution simulations." Earth System Dynamics 10(3): 485-499.

Salzberg, S. L. (1994). "C4.5: Programs for Machine Learning by J. Ross Quinlan. Morgan Kaufmann Publishers, Inc., 1993." Machine Learning 16(3): 235-240.

Schneidewind, T., S. Lee, A. M. Vicedo-Cabrera and A. Saucy (2025). "The risk of hospitalization associated with foehn winds and temperature in the mountainous region of Switzerland." Environmental epidemiology 9(5).

Seibert, P. (1990). "South Foehn Studies since the Alpex Experiment." Meteorology and Atmospheric Physics 43(1-4): 91-103.

Seluchi, M. E., F. A. Norte, P. Satyamurty and S. C. Chou (2003). "Analysis of three situations of the Foehn effect over the Andes (zonda wind) using the Eta-CPTEC regional model." Weather and Forecasting 18(3): 481-501.

Sharples, J. J., G. A. Mills, R. H. D. McRae and R. O. Weber (2010). "Foehn-Like Winds and Elevated Fire Danger Conditions in Southeastern Australia." Journal of Applied Meteorology and Climatology 49(6): 1067-1095.

Shilin, Z., W. Rongke, G. Yanbo, T. Jianlong and S. Zhizeng (1993). "The Foehn in the Middle Range of Taihang Mountain." Meteorological Monthly(02): 3-6+29.

Smolarkiewicz, P. K. and R. Rotunno (1989). "Low Froude Number Flow Past Three-Dimensional Obstacles. Part I: Baroclinically Generated Lee Vortices." Journal of Atmospheric Sciences 46(8): 1154-1164.

Smolarkiewicz, P. K. and R. Rotunno (1990). "Low Froude Number Flow Past Three-Dimensional Obstacles. Part II: Upwind Flow Reversal Zone." Journal of Atmospheric Sciences 47(12): 1498-1511.

Speirs, J. C., D. F. Steinhoff, H. A. McGowan, D. H. Bromwich and A. J. Monaghan (2010). "Foehn Winds in the McMurdo Dry Valleys, Antarctica: The Origin of Extreme Warming Events." Journal of Climate 23(13): 3577-3598.

Stauffer, R., A. Zeileis and G. J. Mayr (2024). "Long-Term Foehn Reconstruction Combining Unsupervised and Supervised Learning." International Journal of Climatology 44(16): 5890-5901.

Takane, Y. and H. Kusaka (2011). "Formation Mechanisms of the Extreme High Surface Air Temperature of 40.9°C Observed in the Tokyo Metropolitan Area: Considerations of Dynamic Foehn and Foehnlike Wind." Journal of Applied Meteorology and Climatology 50(9): 1827-1841.

Wang, H., M. Xue, X. Y. Zhang, H. L. Liu, C. H. Zhou, S. C. Tan, H. Z. Che, B. Chen and T. Li (2015). "Mesoscale modeling study of the interactions between aerosols and PBL meteorology during a haze episode in Jing–Jin–Ji (China) and its nearby surrounding region – Part 1: Aerosol distributions and meteorological features." Atmospheric Chemistry and Physics 15(6): 3257-3275.

Wang, Z., Y. Ding, Y. Zhang, C. Wang, J. Li and Y. Gu (2012). "Feature and Mechanism of the Foehn Weather on East Slope Taihang MountainsI:Statistic Feature." Plateau Meteorology 31(2): 547-554.

Widmer, R. (1966). Statistische Untersuchungen über den Föhn im Reusstal und Versuch einer objektiven Föhnprognose für die Station Altdorf, Dissertationsdruckerei Leemann.

Wiesner, L., H. McGowan, A. Sturman and T. Dale (2024). "Subtropical Foehn Winds, Southeast Queensland, Australia." Journal of Geophysical Research: Atmospheres 129(13): e2023JD040410.

Xianping, X., W. Shuyun and Z. Wei (2020). "Analysis of Foehn Characteristics in Middle Section of Taihang Mountains Based on Background Method." Meteorological Science and Technology 48(03): 433-437.

Yan, H., Y. Ding, P. Li, Q. Wang, Y. Xu and W. Zuo (2017). Mind the class weight bias: Weighted maximum mean discrepancy for unsupervised domain adaptation. Proceedings of the IEEE conference on computer vision and pattern recognition.

Zhang, J., L. Liu, L. Xu, Q. Lin, H. Zhao, Z. Wang, S. Guo, M. Hu, D. Liu, Z. Shi, D. Huang and W. Li (2020). "Exploring wintertime regional haze in northeast China: role of coal and biomass burning." Atmospheric Chemistry and Physics 20(9): 5355-5372.

Zhang, Z., W. Xu, S. Zeng, Y. Liu, T. Liu, Y. Zhang, A. Du, Y. Li, N. Zhang, J. Wang, E. Aruffo, P. Han, J. Li, Z. Wang and Y. Sun (2024). "Secondary Organic Aerosol Formation from Ambient Air in Summer in Urban Beijing: Contribution of S/IVOCs and Impacts of Heat Waves." Environmental Science & Technology Letters 11(7): 738-745.

Zhao, K., N. Li, X. Li, M. Sun, J. Shi, D. An, J. Pu and B. Zheng (2021). "Characteristic analysis of atmospheric diffusion conditions of winter foehn weather process in Urumqi City." Arid Land Geography 44(6): 1534-1544.

Zhong, J., X. Zhang, Y. Wang, J. Wang, X. Shen, H. Zhang, T. Wang, Z. Xie, C. Liu, H. Zhang, T. Zhao, J. Sun, S. Fan, Z. Gao, Y. Li and L. Wang (2019). "The two-way feedback mechanism between unfavorable meteorological conditions and cumulative aerosol pollution in various haze regions of China." Atmospheric Chemistry and Physics 19(5): 3287-3306.

Zhou, X., M. Li, X. Huang, T. Liu, H. Zhang, X. Qi, Z. Wang, Y. Qin, G. Geng, J. Wang, X. Chi and A. Ding (2025). "Urban meteorology–chemistry coupling in compound heat–ozone extremes." Nature Cities: 847–856.

Zumbrunnen, T., H. Bugmann, M. Conedera and M. Bürgi (2009). "Linking Forest Fire Regimes and Climate-A Historical Analysis in a Dry Inner Alpine Valley." Ecosystems 12(1): 73-86.

Supplement

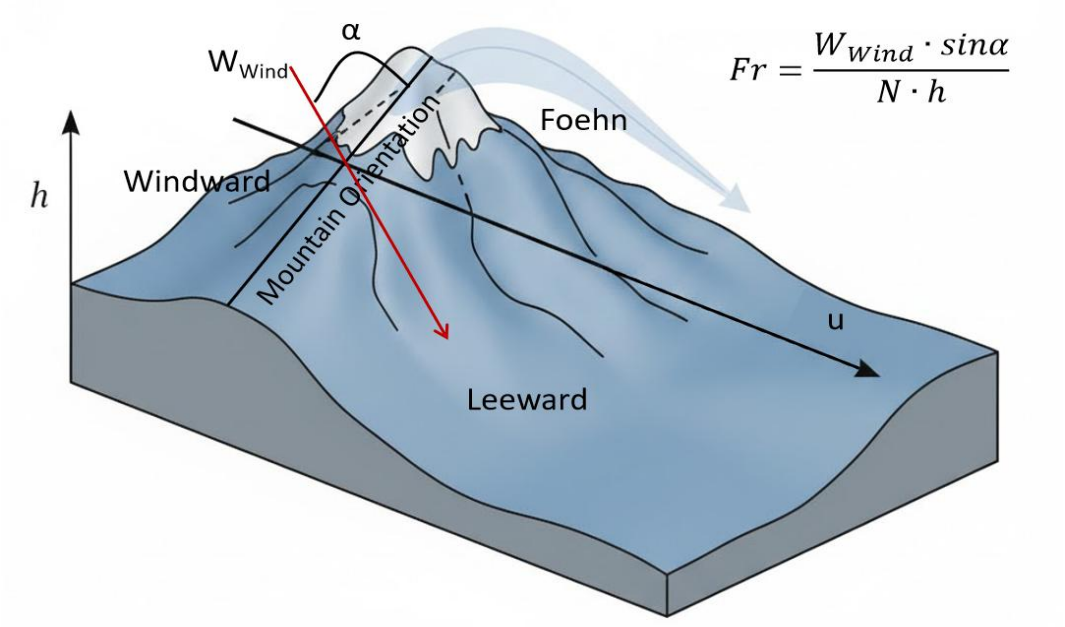

575

Figure S8: Schematic diagram illustrating the Froude number in relation to wind direction when the influence of small-scale terrain on wind direction is neglected. Fr is the Froude number; u is the velocity of the flow normal to the topographic barrier; N is the Brunt Väisälä frequency; h is the height of the topographic barrier; and α is the angle between W_{Wind} and the mountain orientation.

580